Journal Pre-proofs

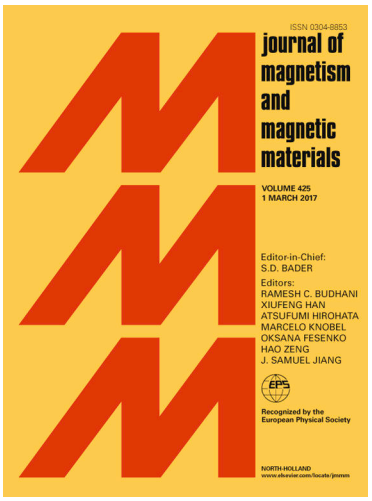

Research articles

Tuning the magnetocaloric response of $Gd_{7-x}Y_xPd_3$ ($2 \leq x \leq 6$) alloys by microstructural modifications

M. Oboz, Z. Śniadecki, P. Zajdel

PII: S0304-8853(21)01041-6
DOI: https://doi.org/10.1016/j.jmmm.2021.168829
Reference: MAGMA 168829

To appear in: *Journal of Magnetism and Magnetic Materials*

Received Date: 27 July 2021
Revised Date: 12 November 2021
Accepted Date: 13 November 2021

Please cite this article as: M. Oboz, Z. Śniadecki, P. Zajdel, Tuning the magnetocaloric response of $Gd_{7-x}Y_xPd_3$ ($2 \leq x \leq 6$) alloys by microstructural modifications, *Journal of Magnetism and Magnetic Materials* (2021), doi: https://doi.org/10.1016/j.jmmm.2021.168829

Tuning the magnetocaloric response of $Gd_{7-x}Y_xPd_3$ ($2 \leq x \leq 6$) alloys by microstructural modifications

M. Oboz[1], Z. Śniadecki[2], P. Zajdel[1]

[1] Institute of Physics, University of Silesia in Katowice, 41-500 Chorzów, Poland
[2] Institute of Molecular Physics, Polish Academy of Sciences, 60-179 Poznań, Poland

Keywords

intermetallics; melt-spun ribbon; magnetic properties; magnetic entropy change; refrigerant capacity

Abstract

We investigated the influence of microstructural changes on the magnetic properties and the magnetocaloric response of the $Gd_{7-x}Y_xPd_3$ ($2 \leq x \leq 6$) alloys rapidly quenched by vacuum suction casting (rc-cast samples) and melt-spinning (melt-spun samples) techniques. Quenched-in structural disorder determines magnetic and magnetocaloric properties in both series of alloys. For the rc-cast samples two distinct magnetic transitions are visible. The peak at higher temperatures is related to the ferromagnetic/paramagnetic transition of the crystalline phase. In contrast, the peak observed at low temperatures is believed to be related to the ferro-para transition of the amorphous phase and/or a spin reorientation. The $Gd_{7-x}Y_xPd_3$ alloys in the form of rapidly cooled cast exhibit the magnetic transition temperatures at 262 K, 242 K, 202 K, 153 K and 9 K, for $2 \leq x \leq 6$ respectively. Curie temperatures of the melt-spun $Gd_{7-x}Y_xPd_3$ alloys are much lower compared to the rc-cast samples. The melt-spun $Gd_5Y_2Pd_3$ orders ferromagnetically below 90 K, while $Gd_4Y_3Pd_3$, $Gd_3Y_4Pd_3$, $Gd_2Y_5Pd_3$ and GdY_6Pd_3 ribbons undergo the magnetic transformation at 65 K, 40 K, 25 K, and 9 K, respectively. Investigated ribbons exhibit almost doubled magnetic entropy change in comparison to the rc-cast samples. For instance, the $-\Delta S_m$ value for melt-spun and rc-cast $Gd_5Y_2Pd_3$ is equal to 6.31 $Jkg^{-1}K^{-1}$ and 3.64 $Jkg^{-1}K^{-1}$, respectively. Moreover, due to the large δT_{FWHM} of the magnetic entropy change peak, both the melt-spun and rc-cast samples exhibit large relative cooling power (*RCP*), reaching 466 Jkg^{-1} ($\Delta\mu_0 H$ = 5 T) for the rc-cast $Gd_5Y_2Pd_3$. *RCP* values are comparable to those of some potential magnetic refrigerants.

1. Introduction

In contrast to the traditional refrigeration technology of compressed gas medium, the magnetic refrigeration is an environmentally friendly technology [1, 2]. The most efficient of the crystalline magnetic alloys exhibiting significant magnetocaloric effect (MCE) show the first order magnetic phase transition (FOMT) with accompanying structural transformation [3-5]. Compared with the FOMT magnetocaloric materials, amorphous alloys exhibit magnetocaloric effect originating from the second order magnetic phase transition (SOMT). Such materials possess unique advantages, as for example superior mechanical properties, low hysteresis losses during magnetization, lack of thermal hysteresis, or better corrosion resistance [6-8]. Moreover, in the recent years, SOMT magnetic materials have been also studied utilizing scaling laws. The existence of different phases in the magnetocaloric composites can affect the magnetocaloric behaviour leading to table-like MCE responses and thus to increase the refrigerant capacity (*RC*) [9, 10]. A recent study of binary (Gd+Gd_7Pd_3 and Gd+GdZn) composite systems show an increase of *RC* value compared to single phase Gd [11-13].

Over the last decades there have been intensive investigations of suitable magnetocaloric materials. A number of them, such as, RE_2ZnMnO_6 (RE = Gd, Dy and Ho) perovskites [14], RE_2FeAlO_6 (RE = Gd, Dy, Ho) oxides [15], Sr_2GdNbO_6 [16], exhibit outstanding magnetocaloric performance.

Recently, complex investigations of the structural, microstructural, magnetic and magnetocaloric properties of the Gd_6YPd_3 alloys utilizing various techniques were performed [17]. The Curie temperature of melt-spun Gd_6YPd_3 has been estimated to be equal to 115 K, although the rapidly cooled cast (rc-cast) sample ordered ferromagnetically at 305 K. The rc-cast Gd_6YPd_3 exhibits $-\Delta S_m$ value of 4.13 $Jkg^{-1}K^{-1}$ and relative cooling power (*RCP*) value of ~805 Jkg^{-1}, for the magnetic field changes of 0-5 T. The structurally disordered Gd_6YPd_3 ribbon exhibits considerable $-\Delta S_m$ value reaching 8.18 $Jkg^{-1}K^{-1}$ and large *RCP* of ~891 Jkg^{-1} [17]. The magnetic and magnetocaloric properties clearly depend on the grain size and varying degree of structural disorder, similarly to the parent Gd_7Pd_3 compound prepared as rapidly cooled cast and in the polycrystalline form [18]. Therefore, we intend to shown the influence of varied kinetics of synthesis process, utilizing different techniques, to study the impact of the microstructural changes and various degree of structural disorder on the magnetocaloric properties of the $Gd_{7-x}Y_xPd_3$ ($2 \leq x \leq 6$) alloys.

2. Experimental details

The rapidly cooled cast (rc-cast) $Gd_{7-x}Y_xPd_3$ alloys were synthesized using the mould casting technique [19]. The applied technology consisted of two steps. First, pure elements were melted

together in an inert gas (argon 5N) atmosphere using a typical arc furnace. In the second step, the obtained ingots were cast in a copper mould using an in-house vacuum suction apparatus. The applied copper mould allowed to obtain bulk rods of 1.5 mm in diameter and about 2 cm in length. The precursor for melt-spinning was initially synthesized by arc-melting. The ingots were subsequently melted in induction furnace and ejected onto the surface of a copper wheel rotating with a surface velocity of 42 ms^{-1}.

The X-ray diffraction (XRD) was used to check the phase composition. Powder diffraction measurements were carried out on a PANalytical PW1050 diffractometer using nickel filtered Cu $K\alpha_{1,2}$ source operating at 30 kV/30 mA. Diffractograms were collected in a step mode with 0.02^o step in an angular range 10-70^o, 24s per point. The incident beam spilled over the sample under 17^o which was later corrected in the refinement. A reference silicon pattern was used to obtain instrumental broadening. Pieces of the rc-casts were ground in an agate mortar and deposited on a double-sided scotch tape attached to a glass slide. Pieces of ribbons of each material, about 2 mm in width and 30 mm in length were deposited on a double-sided scotch tape attached to a glass slide with a shiny (free) side facing the beam.

The microstructural observations and microcompositional analysis were conducted using a JEOL-7600F scanning electron microscope (SEM) equipped with an Oxford energy dispersive X-ray spectroscopy (EDS) microprobe.

The temperature dependences of magnetization were performed using a Quantum Design MPMS-XL-7AC SQUID magnetometer in the temperature range 2-400 K in magnetic fields up to 7 T.

3. Results and discussion

The XRD patterns of the rc-cast of $Gd_{7-x}Y_xPd_3$ ($2 \leq x \leq 6$) alloys are shown in Figure 1a-e. Rietveld refinement [20] was carried out using Fullprof software [21] and was performed in a way described in the previous paper [17]. The starting model for all but one of the compounds was based on a hexagonal Th_7Fe_3-type structure [22] (marked with (I) in Fig 1 and Table 1). One Gd atom (Gd1) was located on Wyckoff site 2b (1/3, 2/3,z) and two Gd atoms (Gd2, Gd3) and one Pd (Pd1) on Wyckoff site 6c (x, -x, z). The acentric $P6_3mc$ space group (No 186) has a floating origin along the z-axis, so the z coordinate of Gd1 atom was fixed at z=0 (1/3, 2/3, 0). The last material in the $Gd_{7-x}Y_xPd_3$ series had a different structure, which was indexed as cubic and later identified as being similar to RE_5Pd_2-type one [23] (marked with (II) in Fig. 1 and Table 1). The refinement of this structure was simplified by locating some atoms on positions with higher symmetry. The final list of atoms for phase II is following: Pd1 32e (x,x,x=0.223), Y1 16c (0,0,0), Y2 8a (1/8, 1/8, 1/8), Y3 48f (x=0.437, 1/8, 1/8). A change of the lattice parameters *a* and *c* of the rc-casts of $Gd_{7-x}Y_xPd_3$

alloys for phases (I) and (II) are shown in Figure 1f. The metallic radius of yttrium and gadolinium are 180 pm and 178.5 pm, respectively. So, the substitution of yttrium should not change significantly the unit cell volume. The lattice parameter *a* of the phase (I) monotonically decreases with increasing yttrium content, while the lattice parameter *c* increases accordingly, with some deviation which is probably caused by the lattice disorder. For the lattice parameter *a* of the phase (II) monotonic decrease is observed (inset in Fig. 1f).

The observed broadening of diffraction lines due to small crystallite size was modelled using formulae developed by Jarvinen [24]. The Thompson-Cox-Hastings function [25] was used as a base profile with instrumental broadening obtained from the Si dataset. A size model 19 appropriate for Laue class 6/*mmm* was chosen with only two spherical harmonics used in the refinement: Y00 (general size) and Y20 (oblate/prolate factor). The obtained profile parameters and a coherent domain size obtained are presented in Table 1.

At the initial stage of refinement for structure (I), all sites were treated as fully occupied either by Gd or Pd. Then test refinements were done in which Y was added to each Gd site with total site occupancy SOF_Gd + SOF_Y constrained 1. It has to be noted that due to nanocrystallinity of the material, reflected in high peak overlap and weak intensities, the stoichiometric part of study can be treated only as an indication. If occupancy refined to more than 1 for Gd or Y it was later constrained at the maximum value. Occupancy preferences obtained in this way are contained in Table 1. For example, in the case of $Gd_5Y_2Pd_3$, the full Gd occupancy was refined for sites Gd1 and Gd2 but came out than 0 for Gd3 indicating that it is most likely occupied by yttrium. This effectively gave a formula $Gd_1Gd_3Y_3Pd_3$, which is reported in Table 1.

For the cubic structure of type (II), compositional refinement was only attempted in the case of GdY_6Pd_3 due to small number of reflections compared to number of parameters. Only Y and Pd were used in the refinement and the chemical occupancies relative to Y3 were found to be Pd1 0.59, Y1 0.48, Y2 0.16, Y3 1.0 (fixed). Therefore the provisional (assuming Y only) stoichiometry was found to be $Y_{9.11}Pd_3$.

Another peak at d-spacing d = 2.76 Å was associated with an impurity observed earlier [17] and it was modelled as a hexagonal Gd/Y - like ($P6_3/mmc$) structure. The mass fraction percentage was refined using the lightest Y-only composition and is reported in Table 1.

Table 1. Profile parameters of the main and secondary phases with an upper estimate of impurity content.

Material	**Parameters of majority phases**				**Minority phases**	
	a (Å)	*c* (Å)	size (nm)	Site pref.	type	mass frac. (%)
$Gd_5Y_2Pd_3$ (I) 92.3 %	9.9659(9)	6.2735(12)	13	Gd, Gd, Y "$Gd_1Gd_3Y_3Pd_3$"	Gd-Y hex	7.7
$Gd_4Y_3Pd_3$ (I) 56 % (II) 35 %	9.9494(6) 13.6732(12)	6.2764(6) --	16 --	--	Gd-Y hex	9
$Gd_3Y_4Pd_3$ (I) 97 %	9.9407(2)	6.2937(3)	27	Gd, Gd, 0.7Y 0.3Gd "$GdGd_{1.6}Y_{4.4}Pd_3$"	Gd-Y hex	3
$Gd_2Y_5Pd_3$ (I) 70 % (II) 25 %	9.9202(3) 13.6401(9)	6.2909(3) --	30 --	--	Gd-Y hex	5
GdY_6Pd_3 (II)	13.6154(2)	--	32	"$Y_{9.11}Pd_3$"	weak peaks	<5%

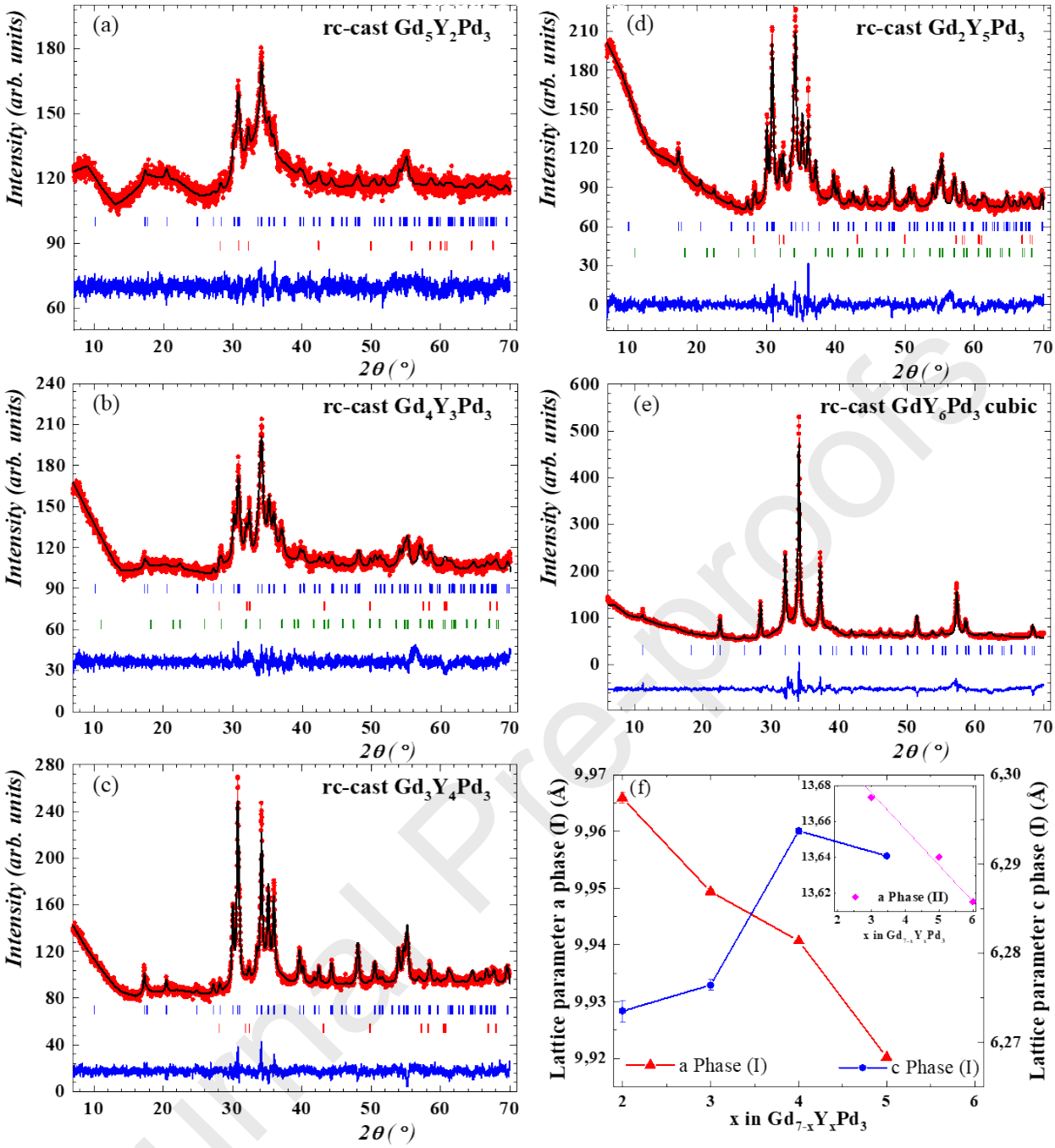

Fig. 1. XRD patterns (a-e) and lattice parameters (f) of the rc-cast $Gd_{7-x}Y_xPd_3$ ($2 \leq x \leq 6$) alloys.

X-ray diffraction patterns collected for $Gd_{7-x}Y_xPd_3$ melt-spun ribbons are shown in Fig. 2 and exhibit dominating contribution of amorphous phase (broad halo). In the case of the $Gd_3Y_4Pd_3$ sample there are no other contributions, similar to the melt-spun Gd_6YPd_3, reported in [17]. The obtained diffraction patterns did not reveal well developed strong Bragg reflections, which excluded Rietveld refinement as a phase identification method. The broad features only point out to a short range periodicity and a standard term of 'a coherent domain size' loses its meaning, since the 'size' obtained from line broadening is of the order of the lattice parameter, as shown in [17]. This is a result of the fact that the crystallite size is below the applicability limit of the Scherrer's formula.

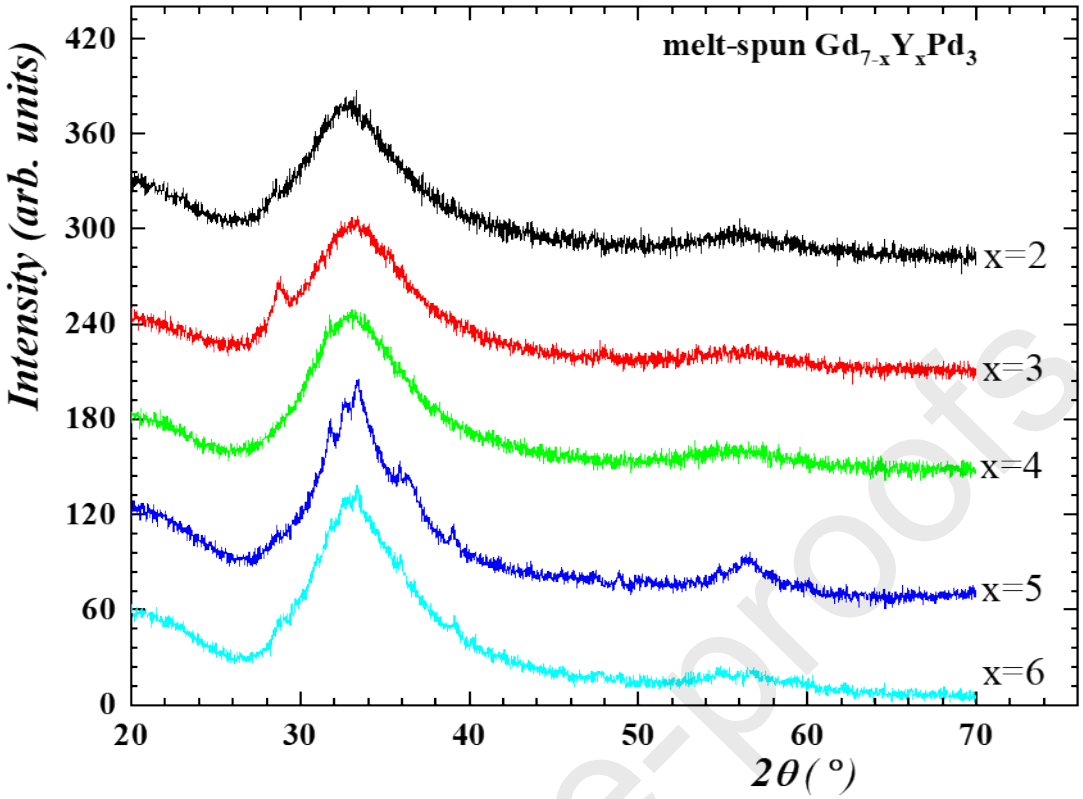

Fig. 2. Overview of the structural evolution of the materials revealing different long range ordered phases for the Yttrium rich (GdY_6Pd_3, $Gd_2Y_5Pd_3$, $Gd_2Y_5Pd_3$) and Gd-rich alloys ($Gd_4Y_3Pd_3$, $Gd_5Y_2Pd_3$).

The extra small reflections are evident for materials with nominal Gd content x = 1, 2, 4, and 5. In materials with $x_{Gd} < 3$ one can notice small peak located at about 2Θ = 39 degrees. For $x_{Gd} > 3$ one observes an extra peak at about 2Θ = 29 degrees. Unfortunately, the identification of this additional phase is impossible from the powder diffractograms due to insufficient number of characteristic peaks. By analogy with results for rc-casts $Gd_{7-x}Y_xPd_3$, the peak located at about 29 degrees (d-spacing d = 3.15 Å) could be associated with a hexagonal Gd/Y - like ($P6_3/mmc$) structure observed earlier [17]. The reflection would then be a (100) peak of this phase and the absence of other peaks would be a direct result of a strong preferred orientation along (100) direction. For materials with $x_{Gd} > 3$, the peak at 2Θ = 39 degrees (d-spacing d = 2.35 Å) might be a (111) from a simple cubic YPd_3-type phase, but also a (002) from a hexagonal GdPd-type phase. Phases that can be excluded comprise Gd_3Pd_2, Y_3Pd, Y_3Pd_2 or YPd.

The SEM micrographs of the rc-cast and melt-spun $Gd_{7-x}Y_xPd_3$ are shown in Figure 3. The SEM/EDS elemental analysis showed that the samples exhibit a single phase microstructure and the stoichiometry was in agreement with the nominal one. Moreover, the SEM analysis of the rc-casts $Gd_{7-x}Y_xPd_3$ samples showed that the materials consist of the nanocrystallites. The cross section of the rc-casts shows parallel arrangement of grains which size is in the range of 23-76 nm (Fig. 3a-e).

The $Gd_2Y_5Pd_3$ and $Gd_3Y_4Pd_3$ samples show the largest grain size. Compared to rc-casts, the cross section of ribbons exhibits a complex morphology consisting of various regions of larger and smaller size.

The SEM micrographs of melt-spun $Gd_{7-x}Y_xPd_3$ ribbons are similar to those obtained earlier for the melt-spun Gd_6YPd_3 one [17]. The Gd_6YPd_3 melt-spun sample exhibited non-crystalline character with small nanocrystals embedded in an amorphous matrix. It seems highly probable that the investigated melt-spun $Gd_{7-x}Y_xPd_3$ ($2 < x < 5$) series is similar in this manner.

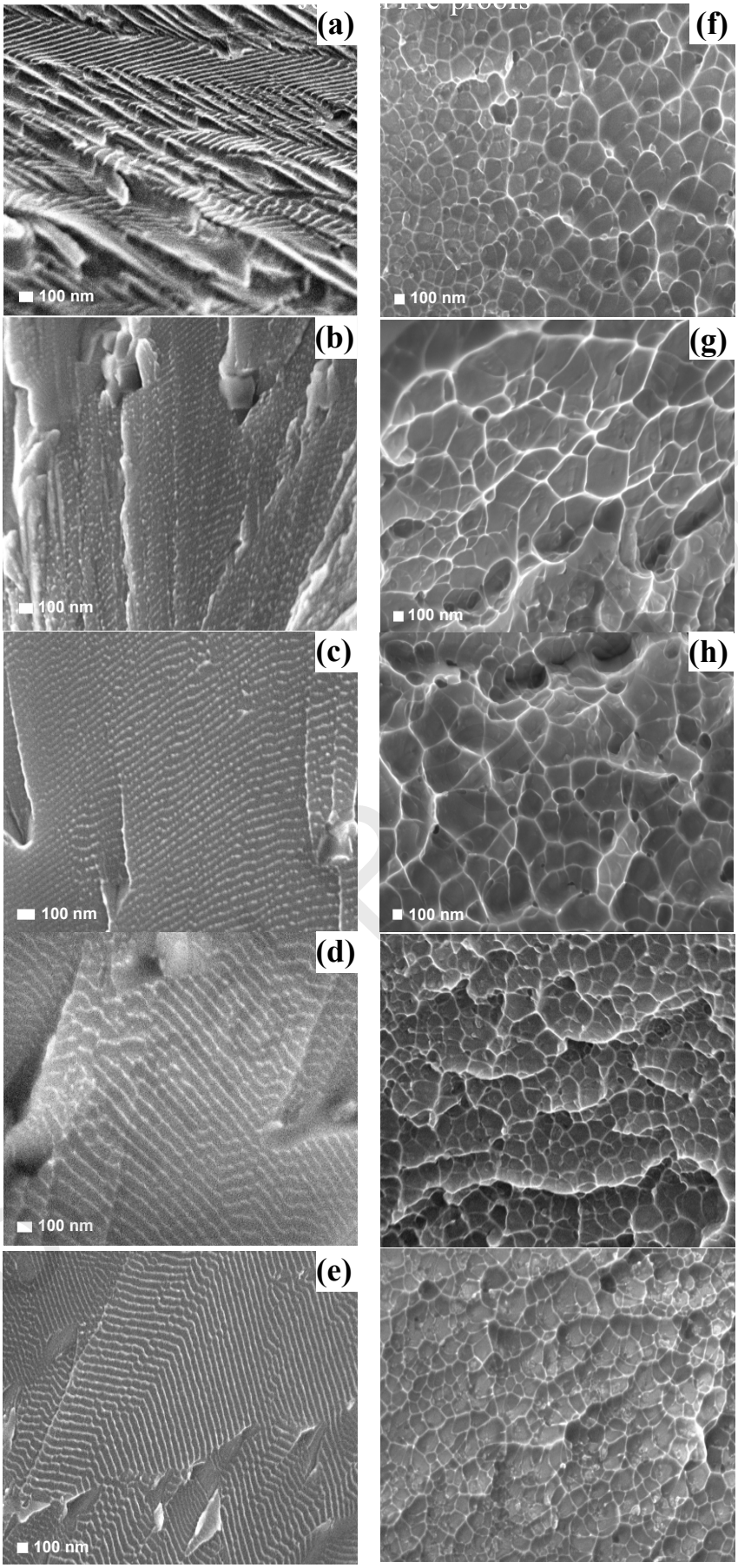

Fig. 3. SEM micrographs of (a) $Gd_5Y_2Pd_3$, (b) $Gd_4Y_3Pd_3$, (c) $Gd_3Y_4Pd_3$, (d) $Gd_2Y_5Pd_3$, (e) GdY_6Pd_3 rc-casts and (f) $Gd_5Y_2Pd_3$, (g) $Gd_4Y_3Pd_3$, (h) $Gd_3Y_4Pd_3$, (i) $Gd_2Y_5Pd_3$, (j) GdY_6Pd_3 melt-spun samples.

Fig. 4 shows temperature dependences of magnetization of rc-cast (Fig. 4a) and melt-spun (Fig. 4c) $Gd_{7-x}Y_xPd_3$, while Figures 4b,d exhibit temperature dependence of dM/dT curves with determined Curie temperatures (T_C) (also summarized in Table 2). It can be seen that the transition temperature decreases for both rc-casts and ribbons as the content of non-magnetic yttrium increases. The long-range magnetic ordering in the Th_7Fe_3 crystal structure is responsible for the magnetic phase transition observed in the rc-casts. For the rc-cast samples two distinct magnetic transitions are visible. The peak at higher temperatures is related to the ferromagnetic/paramagnetic transition of the crystalline phase. In turn, the peak observed at low temperatures is believed to be related to the ferro-para transition of the amorphous phase and/or a spin reorientation in gadolinium sublattice [17,18,26].

As for the rc-cast Gd_6YPd_3, also for the remaining compositions from the investigated $Gd_{7-x}Y_xPd_3$ (x = 2, 3, 4, 5) series, the magnetic transition temperatures are higher than for the corresponding single crystals [22]. The exception is the GdY_6Pd_3 compound, which crystallized in the cubic crystal structure. Higher Curie temperatures of the rc-casts are a consequence of the increasing number of grains, the induced structural disorder and the slightly different local environments of the atoms at the grain boundaries [18,27]. Moreover, the change in the transition temperature of the rc-cast $Gd_{7-x}Y_xPd_3$ series is nonlinear (inset in Fig. 4a). Especially, broad deviation for x = 3, 4, and 5 is observed. The Gd ions in Th_7Fe_3 crystal structure are located in the triangular configuration. The yttrium substitution into the gadolinium positions destroys partly the triangular arrangement of the Gd ions. Thus, with increasing Y-content the lattice disorder starts to have an impact on the magnetic properties and observed increase in T_C suggests stronger coupling between magnetic moments. The T_C values for the ribbons were found to be much lower than for rc-casts. The structural disorder and lack of the long-range interactions in amorphous phase is responsible for this behaviour. For the melt-spun $Gd_{7-x}Y_xPd_3$ ribbons, the Curie temperature dependence is almost linear (inset in Fig.4c). The observed change in the Curie temperature of the ribbons makes it possible to estimate the transition temperature for the parent compound Gd_7Pd_3, for which the value should be approximately 135 K. This value is consistent with that found in the amorphous compound $Gd_{70}Pd_{30}$ [28]. The greatest deviation was observed for x = 4 and for this sample a clear decrease in the magnetization value is also visible. The properties of the ribbons are primarily related to the presence of the amorphous phase, while the deviations are connected with the presence of nanocrystalline phases, their fraction and size.

Table 2. Values of magnetization (at $\mu_0 H$ = 0.1 T) and Curie temperature of the rc-cast and the melt-spun $Gd_{7-x}Y_xPd_3$ alloys.

Compound	Magnetization at $\mu_0 H$ = 0.1 T (μ_B/Gd)		Curie temperature (K)		$(-\Delta S_m)$ (0–5 T) (J kg^{-1}K^{-1})		*RCP* (0–5 T) (J kg^{-1})	
	rc-cast	ribbon	rc-cast	ribbon	rc-cast	ribbon	rc-cast	ribbon
x = 2	2.1	5.9	262	90	3.64	6.31	466	360
x = 3	3.3	5.5	242	65	3.22	6.39	357	269
x = 4	3.6	2.2	202	40	2.87	4.06	350	259
x = 5	3.8	1.7	153	25	1.92	4.84	355	277
x = 6	1	1	9	9	2.32	3.01	118	85

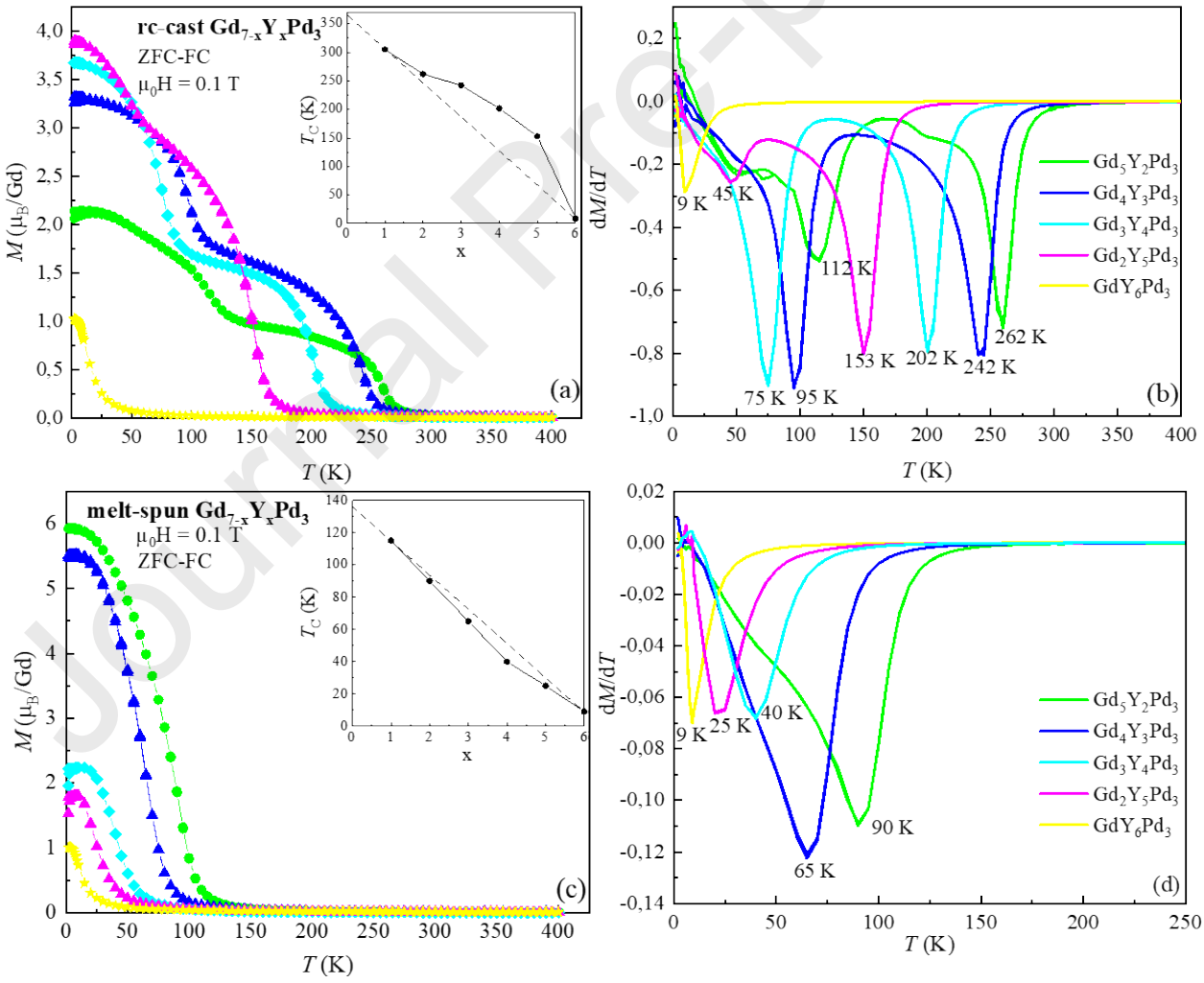

Fig. 4. Thermal variation of magnetization measured in zero field cooled (ZFC) and field cooled (FC) modes ($\mu_0 H$ 0.1 T) (a,c) and dM/dT (b,d) for the rc-cast and the melt-spun $Gd_{7-x}Y_xPd_3$. Insets show the Curie temperatures for the $Gd_{7-x}Y_xPd_3$ series.

The magnetic entropy change (ΔS_m) of all compounds was determined by numerical integration of the Maxwell relation:

$$\Delta S_m(T,\ \Delta H) = \int_{H_1}^{H_2}\left(\frac{\delta M}{\delta T}\right)_H dH\ , \quad (1)$$

from a set of isothermal magnetization curves $M(\mu_o H)$ measured up to $\mu_o H_{max}$ = 7 T.

The relative cooling power (*RCP*) was calculated using following formula:

$$RCP = -\Delta S_{max}\ \delta T_{FWHM} = -\Delta S_{max}(T_2 - T_1), \quad (2)$$

where δT_{FWHM} is the full width at half maximum of the $\Delta S_m(T)$ curve [29].

Fig. 5 shows the temperature dependence of $-\Delta S_m$ under an applied field change of 5 T for the rc-casts and the melt-spun ribbons. For the rc-cast $Gd_{7-x}Y_xPd_3$ (x = 2, 3, 4, 5) samples a table-like magnetocaloric effect in a wide temperature range is observed. Such a table-shaped magneto-caloric effect was earlier observed for other Gd-based compounds [30,31]. For the GdY_6Pd_3 rc-cast the temperature dependence of the magnetic entropy change shows different shape due to dissimilar crystal structure. The table-like behaviour of the temperature dependence of magnetic entropy change ($-\Delta S_m$) is caused by the successive magnetic transitions of crystalline and amorphous phases/or reorientation of magnetic moments in the gadolinium sublattice. The peaks observed at lower temperatures are in agreement with the transition temperatures of the amorphous phase. However, the low temperature peaks of $-\Delta S_m$ may be also caused by the spin reorientation transition which has been reported before in [32-34]. Spin reorientation was previously observed for the monocrystals [22] and the rapidly cooled samples [18] of the $Gd_{7-x}Y_xPd_3$ series. It should also be noted that for x = 5 the ratio of the peaks is the opposite than for the other compositions equal to x = 2, 3, 4, i.e. the high-temperature peak has a greater intensity compared to the low-temperature one. The comparison of the magnetocaloric properties of $Gd_{7-x}Y_xPd_3$ rc-casts series is shown in Fig. 5b,c. For the $Gd_2Y_5Pd_3$ the change in the $-\Delta S_m$ slope (Fig. 5b) at higher values of the magnetic field is clearly visible. The calculated magnetic entropy changes at 5 T for the ribbons are found to be almost doubled when compared with the rc-cast samples (Table 1). For instance, the $-\Delta S_m$ value for the melt-spun and the rc-cast $Gd_5Y_2Pd_3$ is equal to 6.31 $Jkg^{-1}K^{-1}$ and 3.64 $Jkg^{-1}K^{-1}$, respectively (Fig. 5d). The magnetocaloric effect (MCE) weakens with increasing Y content. However, it can be seen that for the $Gd_4Y_3Pd_3$ and $Gd_2Y_5Pd_3$ ribbons the value of the $-\Delta S_m$ is overestimated. Moreover, for samples with x = 3 and 5 a nonlinear change in the $-\Delta S_m$ is observed. For both alloys some Bragg reflections are observed in the XRD diffraction patterns and presence of crystalline phase can result in such behavior.

Due to the large δT_{FWHM} of the magnetic entropy changes peak, both the melt-spun and rc-cast samples exhibit large refrigerant cooling power (*RCP*) (Table 1), reaching 466 Jkg^{-1} ($\Delta\mu_0 H$ = 5 T) for the rc-cast $Gd_5Y_2Pd_3$.

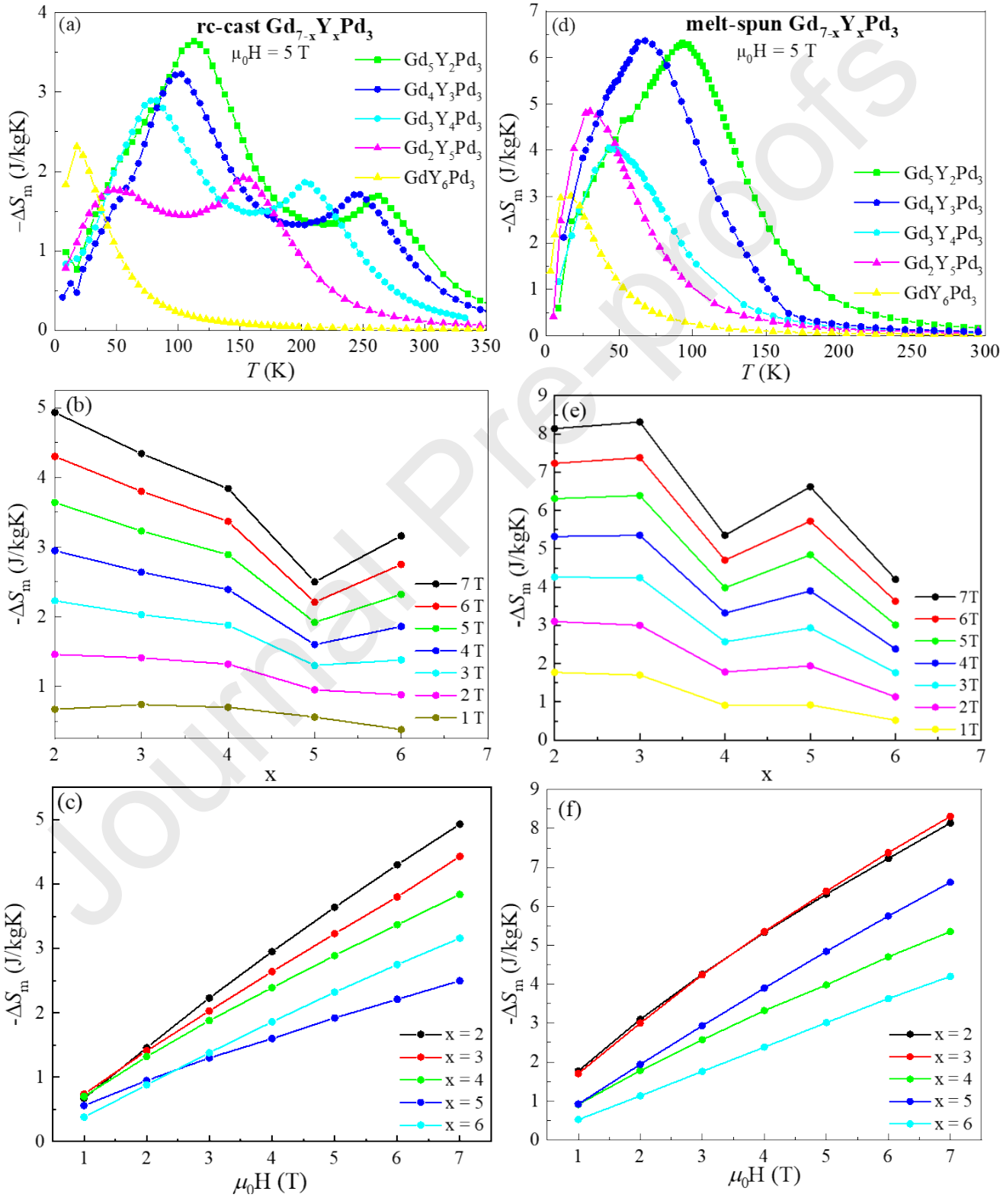

Fig. 5. The comparison of the magnetocaloric properties of the rc-casts (a,b,c) and the melt-spun $Gd_{7-x}Y_xPd_3$ series (d,e,f).

4. Conclusions

The rapidly cooled casts and melt- spun ribbons of $Gd_{7-x}Y_xPd_3$ (x = 2, 3, 4, 5, 6) series were prepared. The exchange *RKKY* interaction between Gd ions is a dominating mechanism being responsible for the magnetic properties of the studied $Gd_{7-x}Y_xPd_3$ rc-casts. Moreover, the yttrium substitution into the gadolinium crystallographic positions partly destroys the triangular arrangement of the Gd ions in the Th_7Fe_3 crystal structure and the lattice disorder influences magnetic properties of Y-rich samples. The Curie temperatures of the melt-spun $Gd_{7-x}Y_xPd_3$ ribbons are lower than for the rc-casts. This behaviour is related to the effect of structural disorder and the lack of long-range magnetic interactions. The magnetic entropy change ΔS_m of the $Gd_{7-x}Y_xPd_3$ (x = 2, 3, 4, 5, 6) ribbons is larger compared to its crystalline counterparts. The table-like magnetocaloric effect in a wide temperature span was obtained for the rc-casts and results in an enhanced δT_{FWHM} and large *RCP* values.

Acknowledgements

This work was financially supported by Polish National Science Centre in frame of Project 2017/01/X/ST3/01838 (MINIATURA 1).

References:

[1] V. Franco, J.S. Blázquez, A. Ingale, B. Conde, The magnetocaloric effect and magnetic refrigeration near room temperature: Materials and models, Annu. Rev. Mater. Res. 42 (2012) 305-342. doi: 10.1146/annurev-matsci-062910-100356

[2] O. Gutfleisch, M.A. Willard, E. Brück, C.H. Chen, S.G. Sankar, J.P. Liu, Magnetic Materials and Devices for the 21st Century: Stronger, Lighter, and More Energy Efficient, Adv. Mater. 23 (7) (2011) 821-842. doi.org/10.1002/adma.201002180

[3] K.A. Gschneidner, Jr., V.K. Pecharsky, A.O. Tsokol, Recent developments in magnetocaloric materials, Rep. Prog. Phys. 68 (2005) 1479-1539. doi:10.1088/0034-4885/68/6/R04

[4] J. Liu, J.D. Moore, K.P. Skokov, M. Krautz, K. Löwe, A. Barcza, M. Katter, O. Gutfleisch, Exploring La $(Fe,Si)_{13}$-based magnetic refrigerants towards application, Scr. Mater. 67 (2012) 584–589. doi.org/10.1016/j.scriptamat.2012.05.039

[5] O. Tegus, E. Brück, K.H.J. Buschow, F.R. De Boer, Transition-metal-based magnetic refrigerants for room-temperature applications, Nature 415 (2002), 150–152.

[6] W. Wang, The nature and properties of amorphous materials, Prog. Phys. 33 (2013), 177–350.

[7] F. Wang, A. Inoue, Y. Han, Excellent soft magnetic Fe-Co-B-based amorphous alloys with extremely high saturation magnetization above 1.85 T and low coercivity below 3 A/m, J. Alloys Compd. 711 (2017), 132–142. doi.org/10.1016/j.jallcom.2017.03.341

[8] P. Kumar, R. Kumar, Magnetocaloric effect and refrigeration cooling power in amorphous Gd_7Ru_3 alloys, AIP Advances 5 (2015), 077125-1-7. doi: 10.1063/1.4926810

[9] R. Caballero-Flores, V. Franco, A. Conde, K.E. Knipling, M.A. Willard, Appl. Phys. Lett. 98 (2011) 102505. doi: 10.1063/1.3560445

[10] J. Y. Law, V. Franco, (2021) Magnetocaloric Composite Materials. Encyclopedia of Materials: Composites. vol. 2, pp. 461–472. Oxford: Elsevier. doi: 10.1016/B978-0-12-819724-0.00038-0

[11] A. Díaz-García, J.Y. Law, P. Gębara, V. Franco, Phase deconvolution of multiphasic materials by the universal scaling of the magnetocaloric effect, JOM 72 (2020), 2845–2852. doi.org/10.1007/s11837-020-04251-z

[12] J.Y. Law, L.M. Moreno-Ramírez, J.S. Blázquez, V. Franco, A. Conde, GdþGdZn biphasic magnetic composites synthesized in a single preparation step: Increasing refrigerant capacity without decreasing magnetic entropy change, J. Alloys Compd. 675 (2016), 244–247. doi: 10.1016/j.jallcom.2016.03.130

[13] P. Gębara, Á. Díaz-García, J.Y. Law, V. Franco, Magnetocaloric response of binary Gd-Pd and ternary Gd-(Mn,Pd) alloys, J. Magn. Magn. Mat. 500 (2020), 166175.doi: 10.1016/j.jmmm.2019.166175

[14] Lingwei Li, Peng Xu, Shuaikun Ye, Yong Li, Guodong Liu, Dexuan Huo, Mi Yan, Magnetic properties and excellent cryogenic magnetocaloric performances in B-site ordered RE_2ZnMnO_6 (RE = Gd, Dy and Ho) perovskites, Acta Materialia, 194 (2020) 354-365. doi.org/10.1016/j.actamat.2020.05.036

[15] Bingbing Wu, Yikun Zhang, Dan Guo, Jiang Wang, Zhongming Ren, Structure, magnetic properties and cryogenic magneto-caloric effect (MCE) in RE_2FeAlO_6 (RE = Gd, Dy, Ho) oxides Ceramics International 47 (2021) 6290–6297. doi.org/10.1016/j.ceramint.2020.10.207

[16] Peng Xu, Zhipan Ma, Pengfei Wang, Haifeng Wang, Lingwei Li, Materials Today Physics 20 (2021) 100470. doi.org/10.1016/j.mtphys.2021.100470

[17] M. Oboz, Z. Śniadecki, P. Świec, P. Zajdel, E. Talik, A. Guzik, Evolution of the magnetic and magnetocaloric properties of Gd_6YPd_3 alloys originating from structural modifications , J. Magn. Magn. Mat., 511 (2020) 167000, doi.org/10.1016/j.jmmm.2020.167000

[18] E. Talik, A. Guzik, M. Oboz, P. Zajdel, G. Ziółkowski, Magnetocaloric and Hopkinson effects in slowly and rapidly cooled Gd_7Pd_3, International Journal of Materials Research 107(1) (2016) 3-12. doi: 10.3139/146.111318

[19] A. Chrobak, M. Karolus, G. Haneczok, Preparation of Fe-Based Bulk Amorphous and Nanocrystalline Alloys by Mould Suction Casting Technique, Solid State Phenom. 163 (2010) 233-238. doi: 10.4028/www.scientific.net/SSP.163.233

[20] H.M. Rietveld, A profile refinement method for nuclear and magnetic structures, J. Appl. Cryst. 2 (1969) 65-71. doi: 10.1107/S0021889869006558

[21] J. Rodriguez-Carvajal, Recent Developments of the Program FULLPROF, in Commission on Powder Diffraction (IUCr) Newsletter (2001), 26, 12-19. (http://journals.iucr.org/iucr-top/comm/cpd/Newsletters/) (version April 2014)

[22] E. Talik, M. Oboz, J. Kusz, A. Winiarski, W. Hofmeister, Magnetic and transport properties of $Gd_{7-x}Y_xPd_3$ (x = 0 - 6) system, Journal of Alloys and Compounds 582 (2014) 718-729. doi: 10.1016/j.jallcom.2013.08.084

[23] M.L. Fornasini, A. Palenzona, Crystal structure of the so-called $R.E._5Pd_2$ compounds, Journal of the Less-Common Metals 38 (1974) 77-82. doi.org/10.1016/0022-5088(74)90205-7

[24] M. Järvinen, Application of symmetrized harmonics expansion to correction of the preferred orientation effect, J. Appl. Cryst. 26 (1993) 525-531. doi: 10.1107/S0021889893001219

[25] P. Thompson, D.E. Cox, J.B. Hastings, Rietveld refinement of Debye-Scherrer synchrotron X-ray data from Al_2O_3, J. Appl. Cryst. 20 (1987) 79-83. doi: 10.1107/S0021889887087090

[26] K.P. Skokov, Yu.S. Koshkid'ko, D.Yu. Karpenkov, A.Yu. Karpenkov, E.M. Semenova, Yu.G.Pastushenkov, Magnetocaloric Effect in Micro- and Nanocrystalline $TbFe_{11-x}Ti$ Intermetallic Compounds, Journal of Physics: Conference Series 144 (2009) 012087. doi:10.1088/1742-6596/144/1/012087

[27] Pedro Gorria, José L Sánchez Llamazares, Pablo Álvarez, María José Pérez, Jorge Sánchez Marcos, Jesús A Blanco, Relative cooling power enhancement in magneto-caloric nanostructured Pr_2Fe_{17}, J. Phys. D: Appl. Phys. 41 (2008) 192003 (5pp). doi:10.1088/0022-3727/41/19/192003

[28] D.J. Griffiths, D.S. Easton, D.M. Kroeger, Critical exponents of amorphous Gd0.70Pd0.30, Phys. Rev. B Condens. Matter., 31(1) (1985) 287-292. doi: 10.1103/physrevb.31.287.

[29] K.A. Gschneidner Jr V.K. Pecharsky, Magnetocaloric materials. Annu. Rev. Mater. Sci. 30 (2000), 387-429. doi.org/10.1146/annurev.matsci.30.1.387

[30] Yikun Zhang, Bingbing Wu, Dan Guo, Jiang Wang, Zhongming Ren, Magnetic properties and promising cryogenic magneto-caloric performances of $Gd_{20}Ho_{20}Tm_{20}Cu_{20}Ni_{20}$ amorphous ribbons, Chin. Phys. B 30 (2021) 017501. doi.org/10.1088/1674-1056/abc0d7

[31] G.L. Liu, D.Q. Zhao, H.Y. Bai, W.H. Wang, M.X. Pan, Room temperature table-like

magnetocaloric effect in amorphous $Gd_{50}Co_{45}Fe_5$ ribbon , J. Phys. D: Appl. Phys. 49 (2016) 055004. doi:10.1088/0022-3727/49/5/055004

[32] W. Yang, J. Huo, H. Liu, J. Li, L. Song, Q. Li, L. Xue, B. Shen, A. Inoue, Journal of Alloys and Compounds 684 (2016) 29-33. doi.org/10.1016/j.jallcom.2016.05.142

[33] Yikun Zhang, Review of the structural, magnetic and magnetocaloric properties in ternary rare earth RE_2T_2X type intermetallic compounds, Journal of Alloys and Compounds 787 (2019) 1173-1186. doi.org/10.1016/j.jallcom.2019.02.175

[34] Lingwei Li, Mi Yan, Recent progresses in exploring the rare earth based intermetallic compounds for cryogenic magnetic refrigeration, Journal of Alloys and Compounds 823 (2020) 153810. doi.org/10.1016/j.jallcom.2020.153810

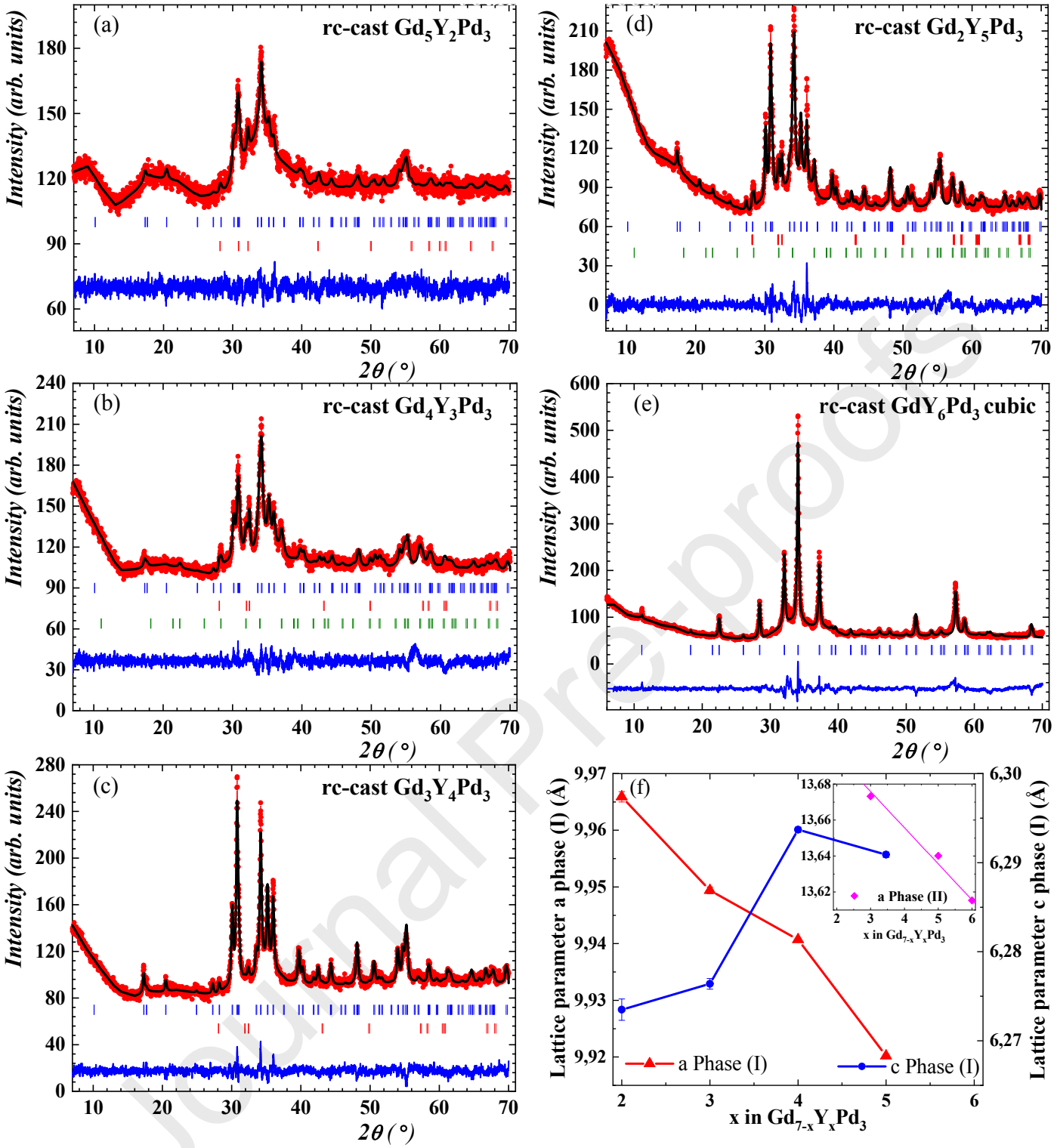

Fig. 1. XRD patterns (a-e) and lattice parameters (f) of the rc-casts of $Gd_{7-x}Y_xPd_3$ ($2 \leq x \leq 6$) alloys.

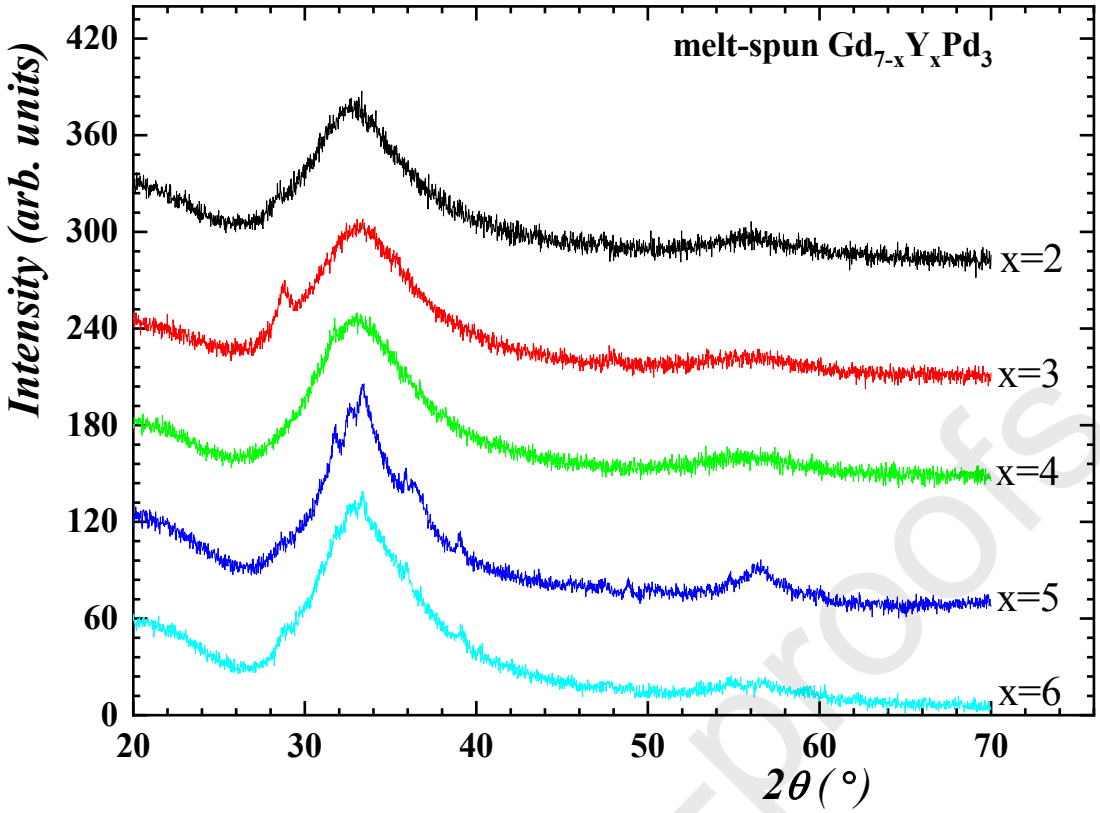

Fig. 2. Overview of the structural evolution of the materials revealed different long range ordered phases for the Yttrium rich (GdY_6Pd_3, $Gd_2Y_5Pd_3$, $Gd_3Y_4Pd_3$) and Gd-rich phases ($Gd_4Y_3Pd_3$,$Gd_5Y_2Pd_3$).

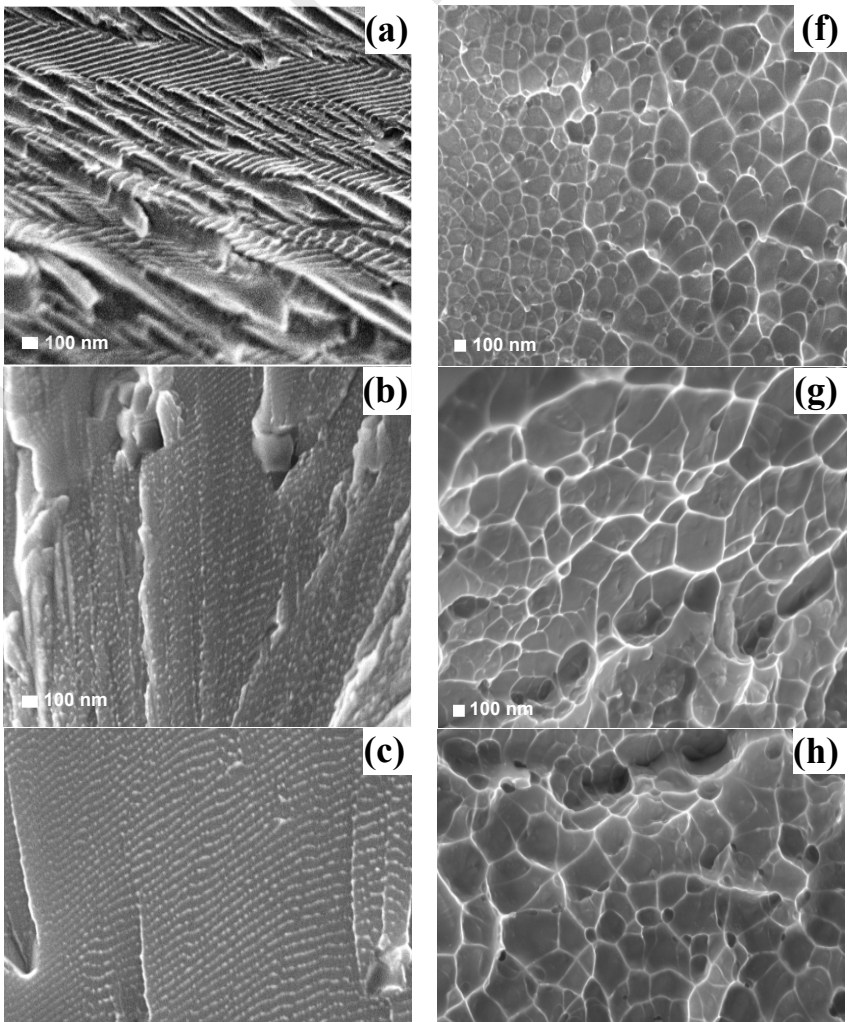

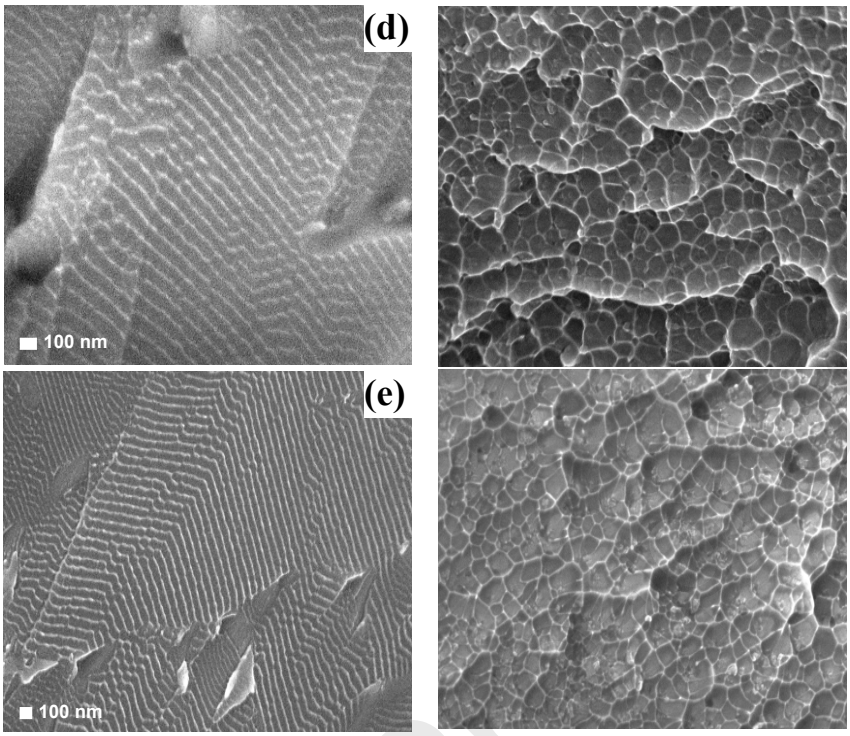

Fig. 3. SEM micrographs of (a) Gd5Y2Pd3, (b) Gd4Y3Pd3, (c) Gd3Y4Pd3, (d) Gd2Y5Pd3, (e) GdY6Pd3 rc-casts and (f) Gd5Y2Pd3, (g) Gd4Y3Pd3, (h) Gd3Y4Pd3, (i) Gd2Y5Pd3, (j) GdY6Pd3 melt-spun.

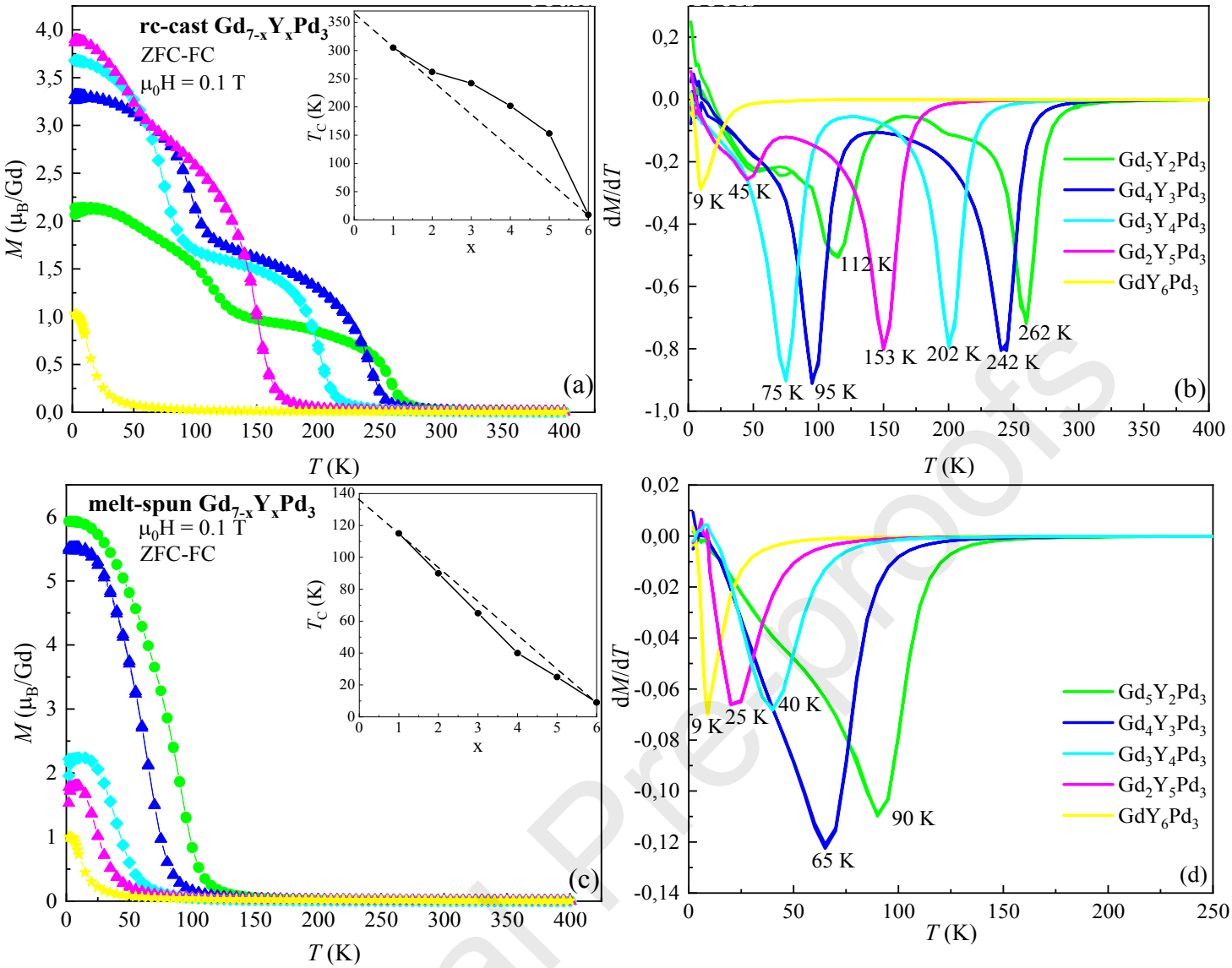

Fig. 4. Thermal variation of magnetization measured in zero field cooled (ZFC) and field cooled (FC) modes in 1 kOe (a,c) and dM/dT (b,d) for rc-cast and melt-spun $Gd_{7-x}Y_xPd_3$. Insets show the Curie temperatures for the $Gd_{7-x}Y_xPd_3$ series.

(c) (d)

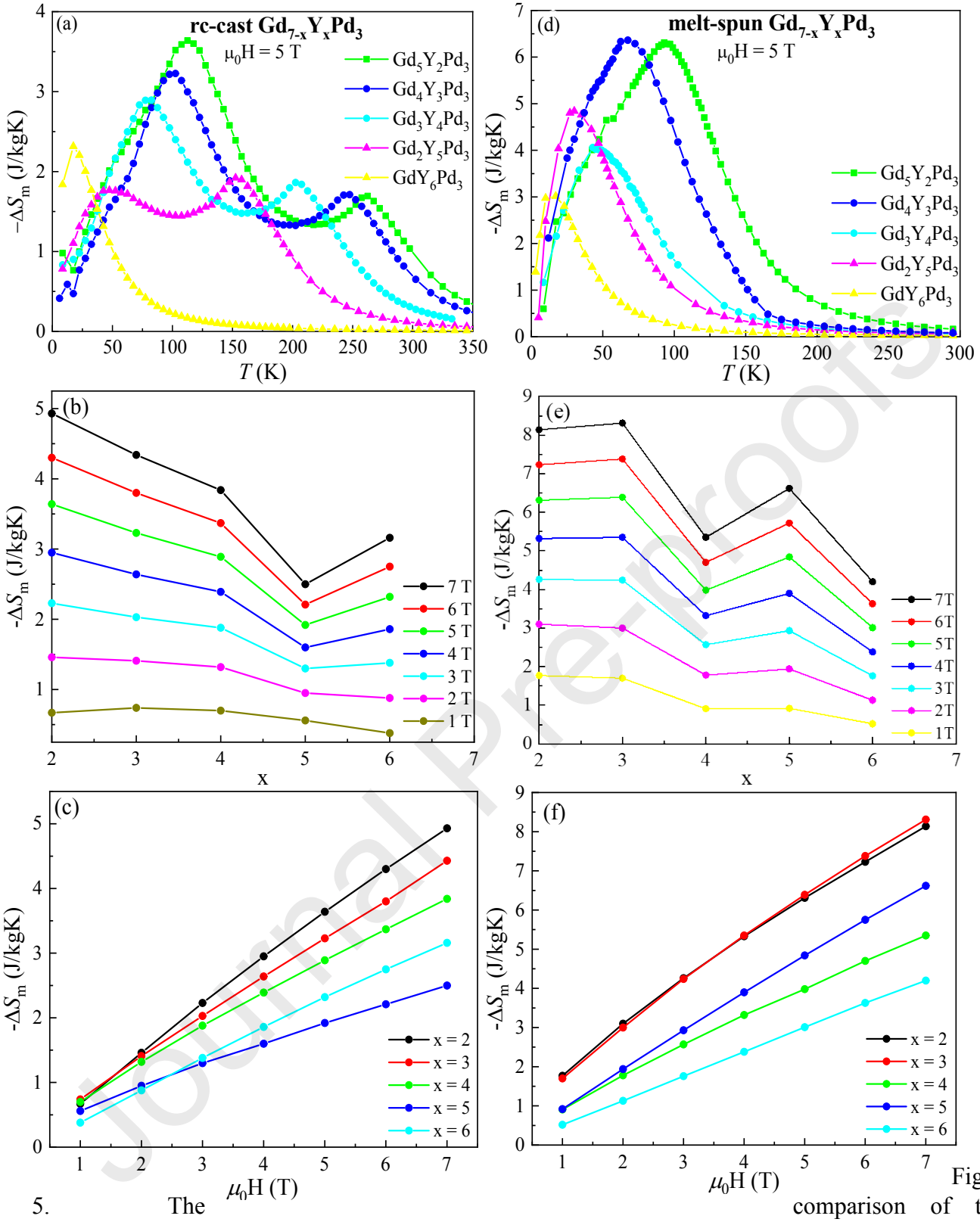

Fig. 5. The comparison of the magnetocaloric properties of rc-casts (a,b,c) and melt-spun $Gd_{7-x}Y_xPd_3$ series (d,e,f).

Table 1. Profile parameters of the main and secondary phases with an upper estimate of impurity content.

Material	Parameters of majority phases	Minority phases

	a (Å)	*c* (Å)	size (nm)	Site pref.	type	mass frac. (%)
$Gd_5Y_2Pd_3$ (I) 92.3 %	9.9659(9)	6.2735(12)	13	Gd, Gd, Y "$Gd_1Gd_3Y_3Pd_3$"	Gd-Y hex	7.7
$Gd_4Y_3Pd_3$ (I) 56 % (II) 35 %	9.9494(6) 13.6732(12)	6.2764(6) --	16 --	--	Gd-Y hex	9
$Gd_3Y_4Pd_3$ (I) 97 %	9.9407(2)	6.2937(3)	27	Gd, Gd, 0.7Y 0.3Gd "$GdGd_{1.6}Y_{4.4}Pd_3$"	Gd-Y hex	3
$Gd_2Y_5Pd_3$ (I) 70 % (II) 25 %	9.9202(3) 13.6401(9)	6.2909(3) --	30 --	--	Gd-Y hex	5
GdY_6Pd_3 (II)	13.6154(2)	--	32	"$Y_{9.11}Pd_3$"	weak peaks	<5%

Table 2. Magnetization (at $\mu_0 H = 0.1$ T) and Curie temperature of rc-cast and melt-spun $Gd_{7-x}Y_xPd_3$ alloys.

Compound	Magnetization at $\mu_0 H = 0.1$ T (μ_B/Gd)		Curie temperature (K)		$(-\Delta S_m)$ (0–5 T) (J kg^{-1}K^{-1})		*RCP* (0–5 T) (J kg^{-1})	
	rc-cast	ribbon	rc-cast	ribbon	rc-cast	ribbon	rc-cast	ribbon
x = 2	2.1	5.9	262	90	3.64	6.31	466	360
x = 3	3.3	5.5	242	65	3.22	6.39	357	269
x = 4	3.6	2.2	202	40	2.87	4.06	350	259
x = 5	3.8	1.7	153	25	1.92	4.84	355	277
x = 6	1	1	9	9	2.32	3.01	118	85

Highlights

- The $Gd_{7-x}Y_xPd_3$ alloys in various forms utilizing mould casting and melt-spinning

- The influence of microstructure on the magnetic and magnetocaloric properties

- Quenched-in structural disorder determines properties in both series of alloys

- For rc-cast samples two distinct magnetic transitions are visible

Declaration of interests

☒ The authors declare that they have no known competing financial interests or personal relationships that could have appeared to influence the work reported in this paper.

☐The authors declare the following financial interests/personal relationships which may be considered as potential competing interests: